ACS OMEGA

Open Access

http://pubs.acs.org/journal/acsodf

Article

Effect of N_2 and CO_2 on the Explosion Properties of High Equivalence Ratios of Hydrogen

Zhenmin Luo, Hao Qi,* Ruikang Li, Tao Wang, Bin Su, Yang Su, and Tianjun Zhang

Cite This: *ACS Omega* 2023, 8, 48304−48316

Read Online

ACCESS | Metrics & More | Article Recommendations

ABSTRACT: The explosion characteristics of premixed gases under different equivalence ratios (1.0−3.0) and inert gas addition (5−20%) are experimentally investigated, and sensitivity analysis of the radical reactions is carried out using the USC Mech II model to analyze the molar fraction of radicals. The results show that at high equivalence ratios, inert gas has little effect on flame stability. The addition of an inert gas reduces the tensile rate in the early stage of flame growth. At high equivalence ratios, CO_2 inhibits explosive flame propagation twice as effectively as N_2. Due to the large heat capacity and chemical kinetic effects, CO_2 has a stronger inhibitory effect on the explosion pressure than N_2, and the inhibition efficiency on the explosion strength is nearly twice that high. To further analyze the effect of different inert gas addition ratios on chemical kinetics, sensitivity analysis, and molar fraction simulations were performed. The thermal and chemical kinetic effects of CO_2 cause later generation of H and OH radicals and the partial chain reaction involving CO_2 causes a lower peak of H radicals than the peak of H radicals generated under an N_2 atmosphere. However, CO_2 is a direct reactant and the third body to produce a small chemical kinetic effect.

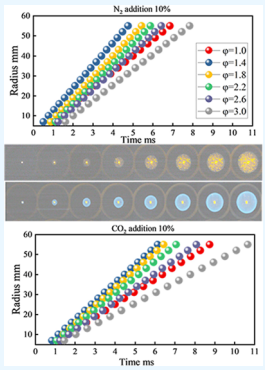

1. INTRODUCTION

As an efficient, low-carbon, clean, and renewable green energy, hydrogen energy plays a vital role as a carrier in the global energy structure transformation, and its demand and application continue to grow.[1−6] According to the International Energy Agency (IEA), the global demand for hydrogen energy has reached 94 million tons in 2021, and according to the current hydrogen development policies formulated by various countries, the global demand for hydrogen is expected to exceed 130 million tons by 2030. By the end of 2020, there were 814 hydrogen refueling stations worldwide. In China, there are 66 hydrogen refueling stations. Hydrogen can be used in both engines and fuel cells, especially in hydrogen fuel cell vehicles, which are an excellent system for utilizing hydrogen as fuel cells produce only water and are highly energy efficient. However, hydrogen has a wide flammability limit (about 4−75% by volume), exceedingly low ignition energy (minimum value of 0.019 mJ), is extremely leaky and brittle, and is highly susceptible to accidental fires and explosions.[7,8]

In recent years, researchers have conducted extensive basic research on hydrogen safety, including ignition limits, ignition locations, initial conditions, and shock waves.[9−14] Zhang et al.[15,16] developed an explosion limit model for combustible gas mixtures and made predictions theoretically. The dependability of the predicted results was tested experimentally, and the effect of blast destabilization on combustible gas mixtures was investigated. Guo et al.[17] and Cao et al.[18] conducted an experimental study of the explosive emissions from hydrogen/air mixtures under counter-ignition, center ignition, and preignition conditions. The results showed that the overpressure, flame spread speed, and flame size were maximum for central ignition and minimum for preignition. Wang et al.[19] experimentally investigated the influence of ignition location on the explosion behavior of hydrogen, comparing the effect of flow field characteristics for central and asymmetric ignition. Huang et al.[20,21] studied that the shock wave strength and flame transmission velocity increased with the initial pressure and that fluid dynamics and thermal instabilities can cause self-accelerated transmission of spherically expanded flames, thereby exacerbating the explosion phenomenon. Hou et al.[22] investigated the blast instability of $CH_4−H_2−O_2$ mixtures at various starting pressures. The results showed that an increase in starting pressure at hydrogen contents below 50% was beneficial in reducing the burst instability of low-hydrogen fuel blends. Bauwens et al.[23−25] investigated the influence of hydrogen concentration and starting turbulence on the explosion pressure and turbulent flame speed of hydrogen. As the hydrogen concentration increased, the maximum pressure increased, and the flame burn speed increased. The growth of the initial turbulence increased the whole speed of flame propagation and maximum overpressure. Rudy et al.[26] studied high-rate turbulent deflagration of premixed hydrogen,

Received: October 2, 2023
Revised: November 3, 2023
Accepted: November 20, 2023
Published: December 6, 2023

https://doi.org/10.1021/acsomega.3c07631
ACS Omega 2023, 8, 48304−48316

the transition process to detonation, and turbulent flame speed rates. Zhang et al.[27] evaluated the dynamical explosion severity of hydrogen in spherical sealed tanks and obtained multidimensional transient explosion characteristics. Grune et al.[28] investigated heterophase hydrogen-air mixtures with a concentration gradient and showed that flames could only speed in the detonation state when the hydrogen concentration was above 20.5%; the detonation speed and pressure of a hydrogen explosion with a concentration gradient were decided by the hydrogen fraction at the top of the tube. Kim et al.[29] carried out a fundamental study of the unexpected explosion behavior of hydrogen-air mixtures in the open field. The results showed that the shock wave strength was influenced by the combustion velocity, volume swelling speed, and flame acceleration; the flame crease increased, the burning velocity increased, and the shock wave increased. In addition, Ma et al.[30] studied the influence of cavities on the transmission behavior of explosive flames and showed that the flame surface area increased due to the growth of vortices and the evolution of turbulence and that the expansion flow from the delayed combustion of the unburned gas in the vortex cavity accelerated the flame leading edge. Wang et al.[31] investigated through numerical simulations and experiments that the explosion flame splits and merges as it passes through a two-channel obstacle, with the maximum velocity first increasing and then decreasing as the block is away from the ignition location. Cao et al.[32] investigated the effect of obstacles on the explosion characteristics of syngas (H_2/CO) under poor ignition conditions and revealed the correlation between flame propagation properties and explosion strength. Luo et al.[33] experimentally investigated the action of a lean hydrogen explosion in a 20L vessel with an opening at one end and explored the influence of gas concentration, exhaust port location, and obstacles on the coupled heat-acoustic-vibration phenomenon in the middle and late stages of the explosion.

Hydrogen explosions can destroy buildings, damage generating equipment, and cause casualties.[34−36] Therefore, the study of hydrogen explosion hazards and their prevention is of great importance for the safe use of hydrogen. Inerting, suppression, and ventilation are common methods to reduce the risk of hydrogen explosions, with inert gases being most commonly used to suppress gas explosions due to their inertness, chemical stability, cleanliness, and effectiveness. N_2 and CO_2 are considered to be the most important explosion suppression gases and are used in many cases to provide an inert environment to prevent further expansion of the explosion. Wang et al.[37] studied the explosion process of H_2-LPG-air mixtures in the presence of N_2 and CO_2 and showed that the addition of the equal volume fraction of CO_2 was more effective in suppressing the explosion. Wang et al.[38] gained the explosion characteristics of hydrogen explosion diluted with Ar, N_2, and CO_2 at subatmospheric pressure and compared the peak explosion pressure, maximum pressure rise rate, and deflagration index. Li et al.[39] studied the influence of inert gases on the bursting of hydrogen clouds by experimental and numerical methods and proposed that inert gases destabilize hydrogen-poor and stoichiometric hydrogen flames. Wei et al.[40] and Zhang et al.[41] studied the effect of N_2 and CO_2 on the suppression of hydrogen flame properties in fixed-volume incendiary bombs and closed channels, respectively, and noted that CO_2 is a superior flame propagation suppressor than Ar and N_2. Li et al.[42] concluded that the thermal diffusion instability of hydrogen-air explosions increases and hydrodynamic instability decreases as the number of CO_2 increases. Yang et al.[43] studied the effects of He, Ar, and N_2 on the flame speed of hydrogen mixtures by varying the ignition location. Zhang et al.[44] studied the multistage inhibition of hydrogen explosion by nonpremixed N_2 and CO_2 in a confined pipeline and concluded that the multistage inhibition effect of same-side retarders was not obvious compared with single-stage inhibition, while the multistage inhibition effect of different-side retarder was the best. Shang et al.[45] experimentally investigated the inferior combustibility limit of H_2−CO mixtures diluted with N_2 and CO_2 at different initial pressures and found that the dilution influence of CO_2 on the inferior combustibility limit was stronger than that of N_2. In addition, the inert gas was found to have a strong influence on the flame structure evolution and the thermodynamic state parameters. Zhang et al.[46] studied the influence of inert gas on the propagation characteristics of H_2/CO/air mixed turbulent premixed flames and found that CO_2 dilution had a more pronounced inhibitory effect on flame radius. Yan et al.[47] experimentally investigated the propagation behavior and explosion pressure characteristics of hydrogen flames near the suppression limit and found that the adiabatic flame temperature, thermal diffusion coefficient, and molar fraction of reactive radicals continued to decrease with increasing CO_2 and N_2 content. Wang et al.[6] experimentally tested the influence of dilute gas on the explosion pressure of hydrogen and calculated the burning heat loss and thermodynamic parameters and found that the influence of dilute gas on the explosion pressure parameters of hydrogen was more significant in the depleted fuel state. Zhang et al.[48] studied the suppression of flame of hydrogen explosions in closed channels by N_2 and CO_2 and found that N_2 and CO_2 inhibited flame velocity and overpressure accumulation. Zhang et al.[49] modeled the ignition behavior of H_2 explosion with He, Ar, N_2, and CO_2 at different equivalence ratios and discussed the thermodynamic and flame kinetic effects of dilution.

So far, there are relatively few studies related to the explosion properties of high equivalence ratio hydrogen premixed gases, the inert gas on the hydrogen-rich conditions of the explosion suppression research needs to be deepened, and the studies on hydrogen explosion have mainly centered on open tanks, but in reality, hydrogen explosions are more prone to occur in confined spaces. Therefore, in this paper, the explosion pressure properties of hydrogen/air premixed gas and inerting laws are studied using a visual spherical explosion experimental system, and high-speed images of the flame propagation process are recorded. Then, the flame propagation velocities under different working conditions were calculated, and the explosion suppression effects of N_2 and CO_2 were analyzed comparatively. Finally, a sensitivity analysis of the relevant radicals (H, OH) was performed based on the USC Mech II model. The pressure characteristics parameters and inerting laws obtained from this test can provide a theoretical basis for the explosion-proof safety design of hydrogen energy-related industries, and a reference for safety management, formulation of emergency measures, and evaluation and audit.

2. EXPERIMENTAL SECTION

2.1. Experimental System. A standard 20L explosive sphere was used for the experiments, consisting mainly of a multichannel gas distribution system, an ignition system, and a data acquisition system. The schematic diagram of the experimental setup is shown in Figure 1. The spherical

https://doi.org/10.1021/acsomega.3c07631
ACS Omega 2023, 8, 48304−48316

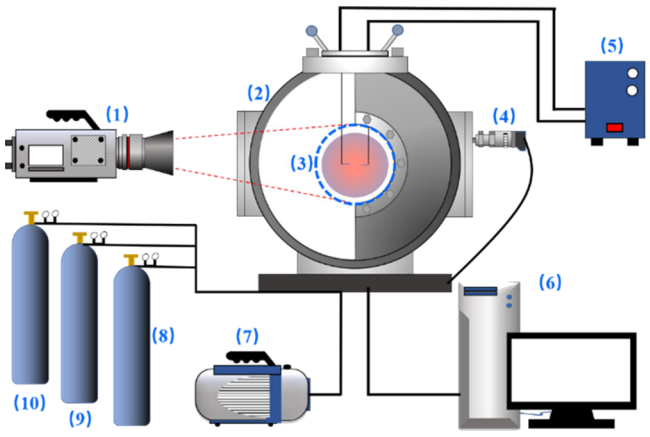

Figure 1. Experimental system ((1) high-speed camera, (2) explosive ball, (3) window, (4) pressure sensor, (5) igniter, (6) computer, (7) vacuum pump, (8) hydrogen cylinder, (9) nitrogen cylinder, and (10) carbon dioxide cylinder).

explosive device has a 110 mm diameter glass sight glass to observe flame propagation. The gas distribution was according to Dalton's law of partial pressure with an accuracy of 0.1%. The ignition device uses a high-pressure pulse ignition with an ignition energy of 0.18 J. The ignition electrode is located at the geometric center of the 20 L ball with a positive and negative spacing of 3.0 mm. The pressure value is collected using a high-frequency pressure sensor with a range of −0.1 to 2.0 MPa, a data collection interval of 0.2 ms, and a resolution of 0.001 MPa. A high-speed camera (USA Vision Research Company, 1.2 megapixels) was used to collect photographs of the blast process at a camera frame rate of 5000 fps. The image information such as the flame radius and flame area of the flame pictures was obtained by the MATLAB program written.

2.2. Experimental Conditions. All experiments were performed at ambient pressure (1.0 atm) and temperature (298 K). The hydrogen equivalence ratio φ is the ratio of the theoretical air volume required for the complete combustion of hydrogen to the actual air volume supplied:

$$\varphi = V_{Air}/(1 - V_{H_2} - V_{Inert}) \quad (1)$$

where V_{H2} and V_{Inert} represent the volume fractions of hydrogen and inert gas in the premixed gas, respectively. V_{Air} denotes the theoretical amount of air required for the complete combustion of hydrogen. The detailed gas compositions are listed in Table 1. In the experiments, the volume fractions of N_2 (or CO_2) were 5, 10, 15, and 20% respectively.

2.3. Parameter Definitions. The propagation speed of the stretched flame in a ball-shaped diffusion flame is[36]

$$S_b = dRa/dt \quad (2)$$

In eq 2, Ra is the flame radius in the photo and t is the time. The area equivalence flame radius is given by eq 3.

$$Ra = \sqrt{A/\pi} \quad (3)$$

where A is the flame area. The burning rate of the flame is affected by the strain and tensile rate of the flame surface. The tensile rate is calculated as

$$\alpha = \frac{1}{A}\cdot\frac{dA}{dt} = \frac{2}{Ra}\cdot\frac{dRa}{dt} = \frac{2}{Ra}\cdot S_b \quad (4)$$

According to the Markstein length theory, there is a linear correlation between the unstretched laminar flame transmission speed S_b^0 and the stretched flame transmission speed S_b of spherical expanding flame.[50]

$$S_b^0 - S_b = L_b\alpha \quad (5)$$

where L_b is the Markstein length and α is the flame stretch rate. S_b^0 can be obtained by extrapolating the S_b in eq 5 to α = 0, The negative value of slope L_b of the fitting line S_b−α is the Markstein length after the gas reaction, which reflects the sensitivity of the flame to stretching and characterizes the flame stability. When $L_b > 0$, it means that the flame transmission speed decreases with the increase of stretching, the prominent flame transmission speed will be suppressed and the flame will stabilize.

The laminar transmission speed of flame is calculated as follows:[51]

$$S_L = \rho_b S_b^0/\rho_u \quad (6)$$

In eq 6, ρ_b and ρ_u are the densities of combusted and uncombusted gas, respectively. Calculation of ρ_b and ρ_u using the Chemkin-Premix code.

The deflagration index K_G is the rate of increase in pressure for the combustion and explosion of an equivalence volume of gas in a container.[52]

$$K_G = (dP/dt)_{max}\cdot\sqrt[3]{V} \quad (7)$$

Table 1. Percentage of Each Component in Premixed Gas[a]

φ	1.0					1.4				
H_2%	29.58	28.10	26.62	25.14	23.66	37.03	35.18	33.32	**31.47**	29.62
N_2%/CO_2%	0	5	10	15	20	0	5	10	15	20
air%	70.42	66.9	63.38	59.86	56.34	62.97	59.82	56.68	53.53	50.38
φ	1.8					2.2				
H_2%	43.05	40.90	38.75	36.59	31.44	48.02	45.62	43.22	40.82	38.42
N_2%/CO_2%	0	5	10	15	20	0	5	10	15	20
air%	56.95	54.1	51.25	48.41	48.56	51.98	49.38	46.78	44.18	41.58
φ	2.6					3.0				
H_2%	52.2	49.59	46.98	44.37	41.76	55.75	52.96	50.18	47.39	44.6
N_2%/CO_2%	0	5	10	15	20	0	5	10	15	20
air%	47.8	45.41	43.02	40.63	38.24	44.25	42.04	39.82	37.61	35.4

[a]The purity of the H_2, CO_2, and N_2 gases used is >99.9%. The main goal of each working condition is to study the influence of dilute gas on hydrogen explosion at high equivalence ratios.

https://doi.org/10.1021/acsomega.3c07631
ACS Omega 2023, 8, 48304−48316

where K_G is the deflagration index, $(dP/dt)_{max}$ is the maximum pressure growth rate, and V is the vessel volume, taken as 0.02 m^3 in this paper.

3. RESULTS AND ANALYSIS

3.1. Flame Characteristics. Figure 2 shows the basic process of flame development in a premixed gas explosion at a

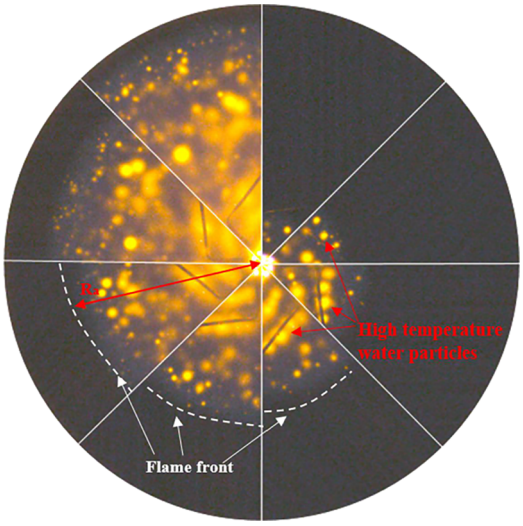

Figure 2. Sketch of the explosion flame development process.

hydrogen equivalence ratio of 1.0. For simplicity, a few specific moments were chosen to illustrate the flame propagation process in a confined space. After successful arc ignition, the flame spreads rapidly, with the flame front separating the already and unburned gas bodies and the energy generated by combustion spreading continuously by heat conduction, thermal convection, and thermal radiation, leading to a gradual increase in the flame radius. At the same time, the total energy in the space accumulates as the oxidation reaction proceeds and the energy spreads. At 3.2 ms the flame radius is 40 mm, and at 4.8 ms the flame spreads to the edge of the window; throughout the process, the spherical flame structure expands and the flame brightness gradually increases.

Figure 3 shows the flame propagation of hydrogen explosions with V_{Inert} = 5, 10, 15, and 20% N_2 (or CO_2) and hydrogen equivalence ratios of φ = 1.0, 1.4, 1.8, 2.2, 2.6, and 3.0. The inhibition effect of inert gases on hydrogen explosions is mainly due to the influence of flame brightness, propagation rate, and flame structure. The brightest explosion flame is obtained for the same V_{Inert} of N_2 or CO_2, with an equivalence ratio of φ = 1.4, indicating that the oxidation reaction is most intense in a constant volume space at φ = 1.4. As φ exceeds 1.4, the explosion flame luminance diminished with increasing φ. At the same V_{Inert}, the explosion flame luminance decreases with increasing V_{Inert}, which indicates that the more inert gas is added, the lower the explosion intensity. When φ = 1.0, the time to grow the flame radius to 40 mm was 4.8 5.0, 5.2, and 6.8 ms for the addition of 5, 10, 15, and 20% N_2, respectively, which were 1.50, 1.56, 1.63, and 2.13 times longer than the pure hydrogen explosion at φ = 1.0. At φ = 1.0 with 5, 10, 15, and 20% CO_2 added, the time to grow the flame radius to 40 mm was 5.0 7.8, 9.8, and 11.6 ms, respectively, 1.56, 2.44, 3.06, and 3.63 times that of a pure hydrogen explosion at φ = 1.0. This indicates that the inert gas has a significant inhibitory

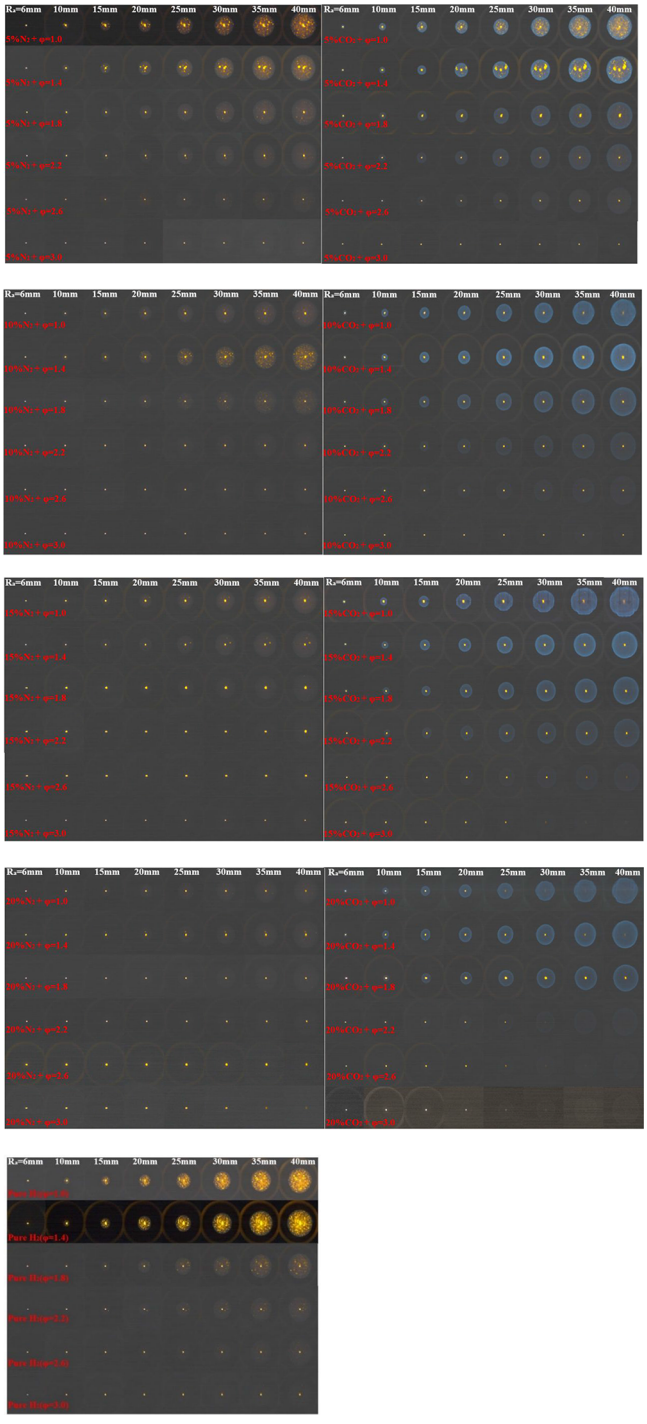

Figure 3. Flame propagation processes.

effect on the flame propagation velocity, which is more pronounced for CO_2 compared to N_2. Furthermore, it can be observed that the fold at the leading edge of the explosion flame changes significantly after the addition of CO_2. Studies of the effect of CO_2 on hydrogen explosions by Li[42] have shown that under hydrogen-rich conditions, the number of cracks in the flame remains constant and the flame surface is smooth. There are two usual reasons for the appearance of folds on the flame front: one is the influence of the ignition electrode, but the ignition electrode only has an effect when the radius is small; The second is caused by the instability of the constant expansion flame, specifically due to the pressure gradient on

https://doi.org/10.1021/acsomega.3c07631
ACS Omega 2023, 8, 48304−48316

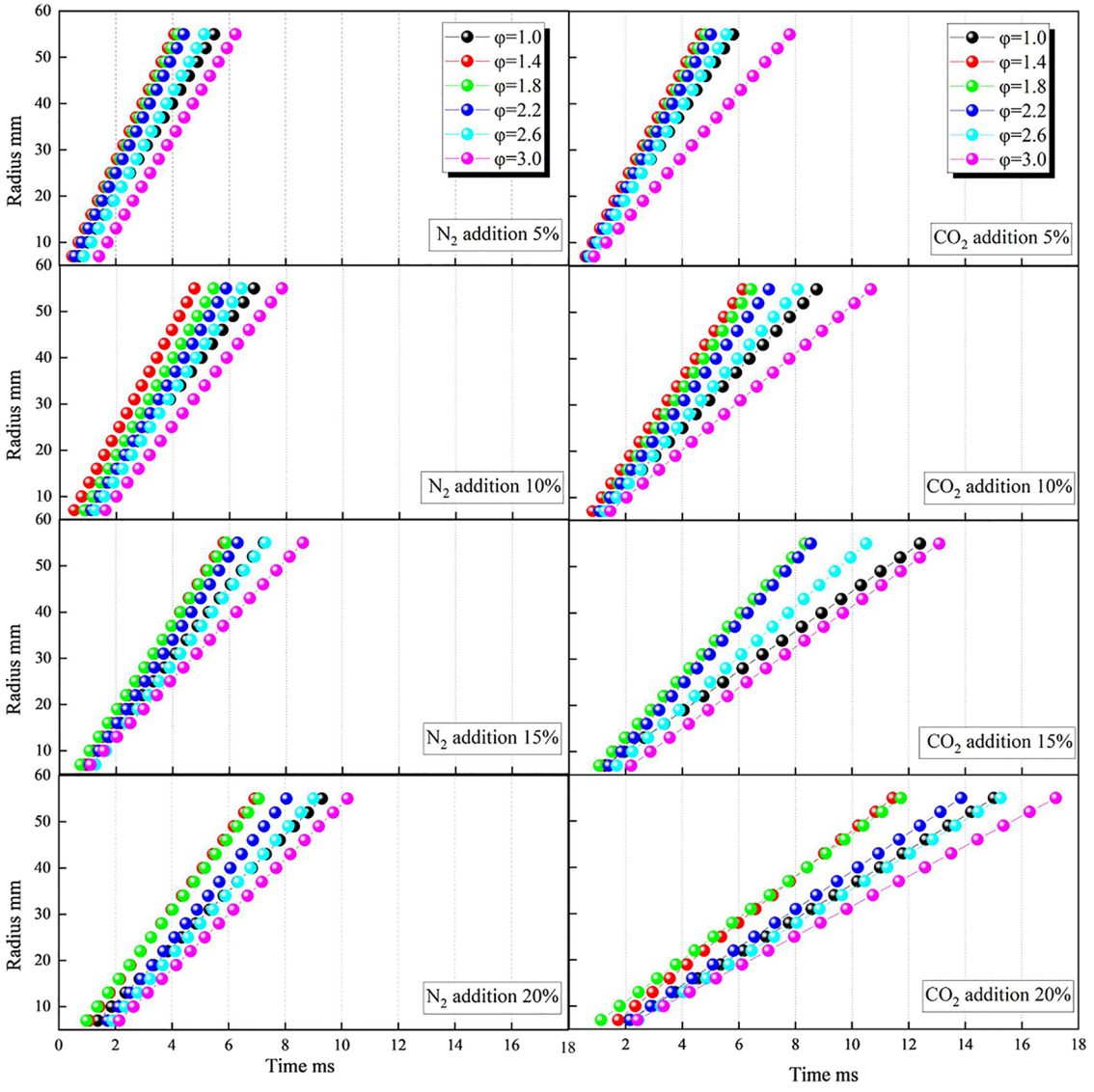

Figure 4. Curve of explosion flame radius with time.

the flame front and the oblique pressure torque generated by the action of the density gradient on the vertical flame surface.

The stronger the flame instability, the more oblique pressure torque generated and the denser the folds on the front surface. It is clear from the images of the exploding flame after the addition of CO_2 that the flame front folds are densest at φ = 1.0 for the same V_{Inert}; As φ increases, the flame front folds gradually decrease. This indicates that in the fuel-rich state the flame instability is reduced by the increase in the amount of hydrogen. For the same V_{Inert}, the more inert gas is added in the range of 5−20%, the smaller and more numerous the explosion flame front folds are, indicating that the increase in inert gas addition increases the flame instability.

Based on the Matlab processing results of the flame image, a graph of the flame radius as a function of time is obtained, as shown in Figure 4. The spherical flame is initially affected by the energy emitted by the ignition electrode, which is eliminated when the flame radius is greater than 6 mm.[53,54] The effective flame radius selected for this test was 6 to 55 mm, and the analysis error is within 3%.

As can be seen in Figure 4, the premixed gas explosion flame radius is linear with time for different V_{Inert} and for different φ. Under the same φ conditions, the more N_2 or CO_2 added, the longer the time required for the explosion flame radius to reach the maximum radius, indicating that there is still a positive correlation between the inhibition of explosion flame propagation by an inert gas under hydrogen-rich conditions. Under the same conditions of V_{Inert}, the suppression effect of CO_2 on the radius of propagation of the explosion flame was significantly better than that of N_2. The development of the radius of the explosion flame with the addition of 10% CO_2 was close to that with the addition of 20% N_2. The flame radius of the explosion flame with the addition of 20% N_2 was also close to that with the addition of 20% CO_2. With the addition of 10% CO_2, the time required for the explosion flame to reach its maximum radius was significantly longer than that required with the addition of 20% N_2 at the same φ, indicating that the inhibitory effect of CO_2 on the flame propagation rate was twice as great as that of N_2 under hydrogen-rich conditions. In addition, with the same increase in the amount of inert gas, CO_2 exhibits a better suppression effect. For example, the time for the flame to grow to its maximum radius increases by a factor of about 1.75 for an increase in the addition of N_2 from

https://doi.org/10.1021/acsomega.3c07631
ACS Omega 2023, 8, 48304−48316

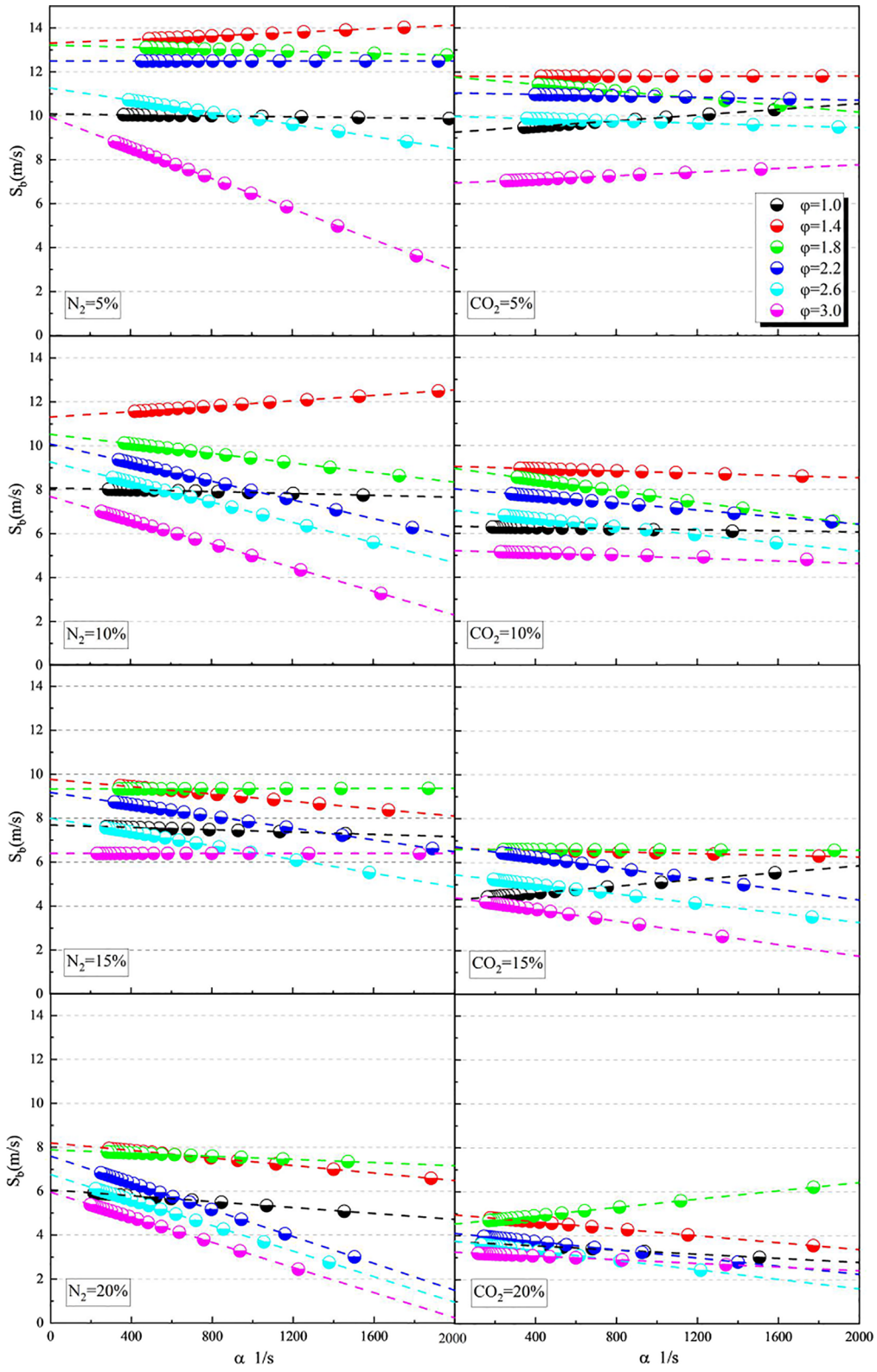

Figure 5. Variation of the tensile flame propagation velocity with tensile rate.

5 to 20% at a = 1.4, and the time required for the flame radius with the addition of CO_2 increases by a factor of 2.4.

The relationship between the propagation velocity S_b of the stretching flame and the stretching rate α is given by eqs 5 and 6. Figure 5 shows the relationship between S_b and α for hydrogen explosion under the inert gas addition conditions. In the initial stages of flame development, the flame radius is small and α is large. As the flame radius increases, the stretching of the flame front essentially continues to diminish. There is an approximately linear relationship between S_b and α. The unstretched flame propagation velocity S_l can be gained by extrapolating S_b to α = 0. The slope of the straight line

https://doi.org/10.1021/acsomega.3c07631
ACS Omega 2023, 8, 48304−48316

obtained from the fit of S_b and α is the negative value of the combustion gas Markstein length L_b. As the inert gas addition ratio increases, the absolute value of the slope of the $S_b-\alpha$ straight line does not change much, i.e., L_b does not change much, which indicates that the effect of inert gas on flame front stability is not significant when V_{Inert} < 20%. The inert gas reduces the rate of propagation of the stretching flame and decreases the rate of stretching in the early stages of the explosion. The higher the specific gravity of the dilute gas, the lower the initial stage stretching rate.

The unstretched flame propagation speed S_l was gained from the intercept of the fitted line in Figure 5 for different conditions, as shown in Figure 6. The upstretched flame propagation speed S_l tends to increase and then decrease with the increase of φ, and the upstretched flame propagation speed is maximum when φ = 1.4. As V_{Inert} increases, S_l decreases. Comparing the suppression of the upstretched flame propagation velocity by N_2 and CO_2, it can be seen that the suppression of inert gas is greatest in the φ range of 1.4−1.8, while it becomes significantly less at φ = 1.0 and 3.0.

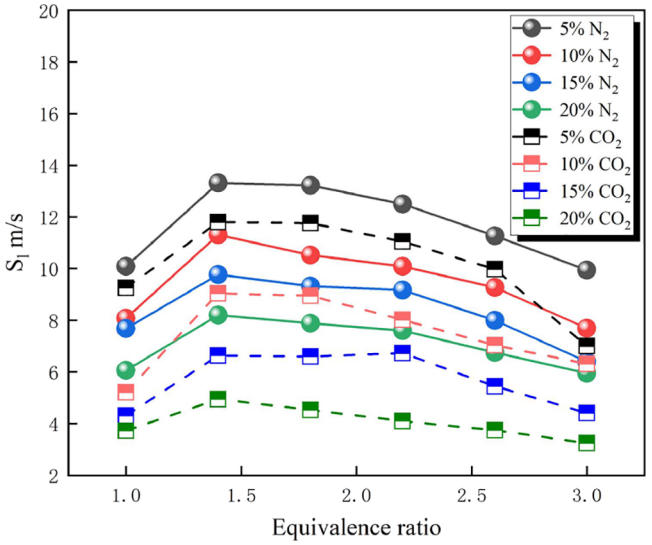

Figure 6. Unstretched flame velocity.

Figure 7 shows a line graph of the laminar flame propagation velocity U_L. The experimental results are calculated according to eq 6. As can be seen from Figure 7, both the experimental results and the numerical calculations show that U_L becomes smaller with increasing V_{Inert}, in an essentially linear relationship. The U_L of hydrogen explosion does not vary much at different V_{Inert} for 1.4 < φ < 2.2. The combustion mechanism used in the flame simulation module is based on USC Mech II proposed by Hai Wang.[55] Hai's mechanism was chosen because it updates the rate coefficients, third-body efficiencies, and radical generation enthalpies, improves the overall combustion characteristics including ignition delay, laminar flame velocity, and the accuracy of predictions of detailed species distributions in the flame and flow reactor, and is thoroughly tested by comparing the calculated kinetic results with experiment. Figure 7 shows that the simulated calculated laminar flow combustion velocities agree well with the experimental results, indicating the high reliability of the experimental results.

3.2. Pressure Characteristics. Figure 8 shows the explosion pressure variation curves for various φ values and

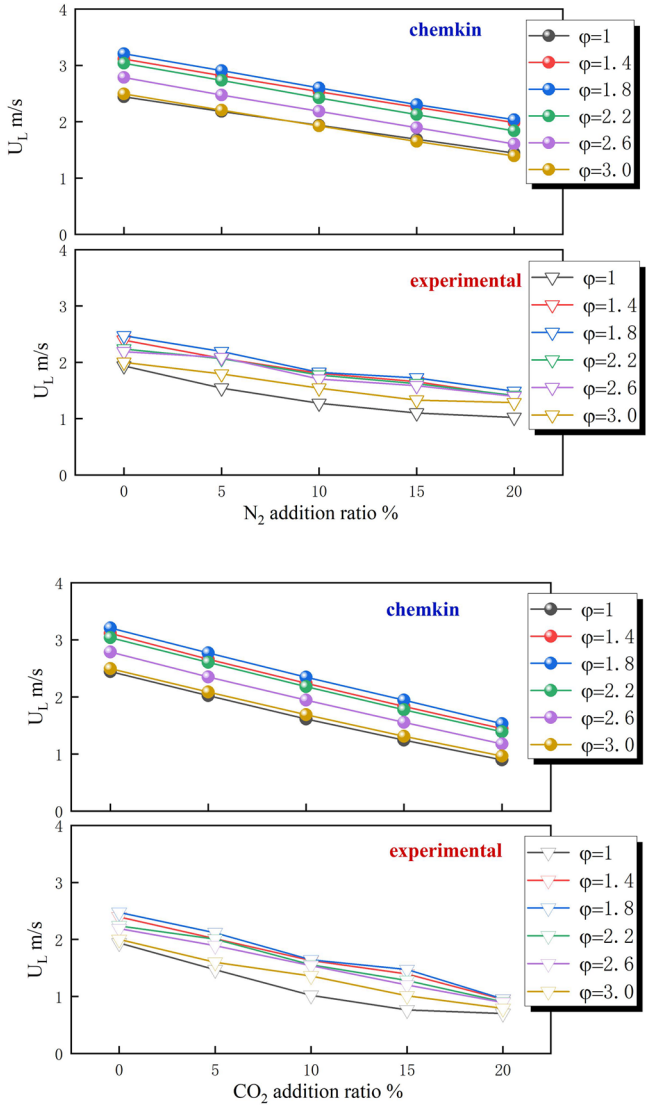

Figure 7. Experimental and simulation results for laminar flame velocity U_L.

different V_{Inert}. The pressure evolution process can be classified into a steady pressure phase and a pressure accumulation process. In the steady pressure phase, the pressure inside the constrained sphere is maintained at a starting value and the flame properties are solely influenced by the starting conditions of the mixture. In the build-up phase, the pressure accumulation is due to the continuous oxidation reaction. As V_{Inert} increases, the duration of the constant pressure phase increases significantly, as does the appearance of the peak pressure. After φ > 1.4, the duration of the constant pressure phase increases with increasing φ.

Figure 9 shows the variation of the maximum explosion pressure and the time to the maximum pressure rise rate for premixed gases as a function of φ and V_{Inert}. As φ increases, the maximum explosion pressure decreases gradually with the addition of inert gas with different V_{Inert}, values and the pressure reduction rate increases continuously. From Figure 9a, b, the law of variation of the pressure peak can be seen as follows: the maximum value of the peak explosion pressure with the addition of 5% N_2 is 0.853 MPa. Pressure peaks with the addition of 20% N_2 are greater than the explosion pressure

https://doi.org/10.1021/acsomega.3c07631
ACS Omega 2023, 8, 48304−48316

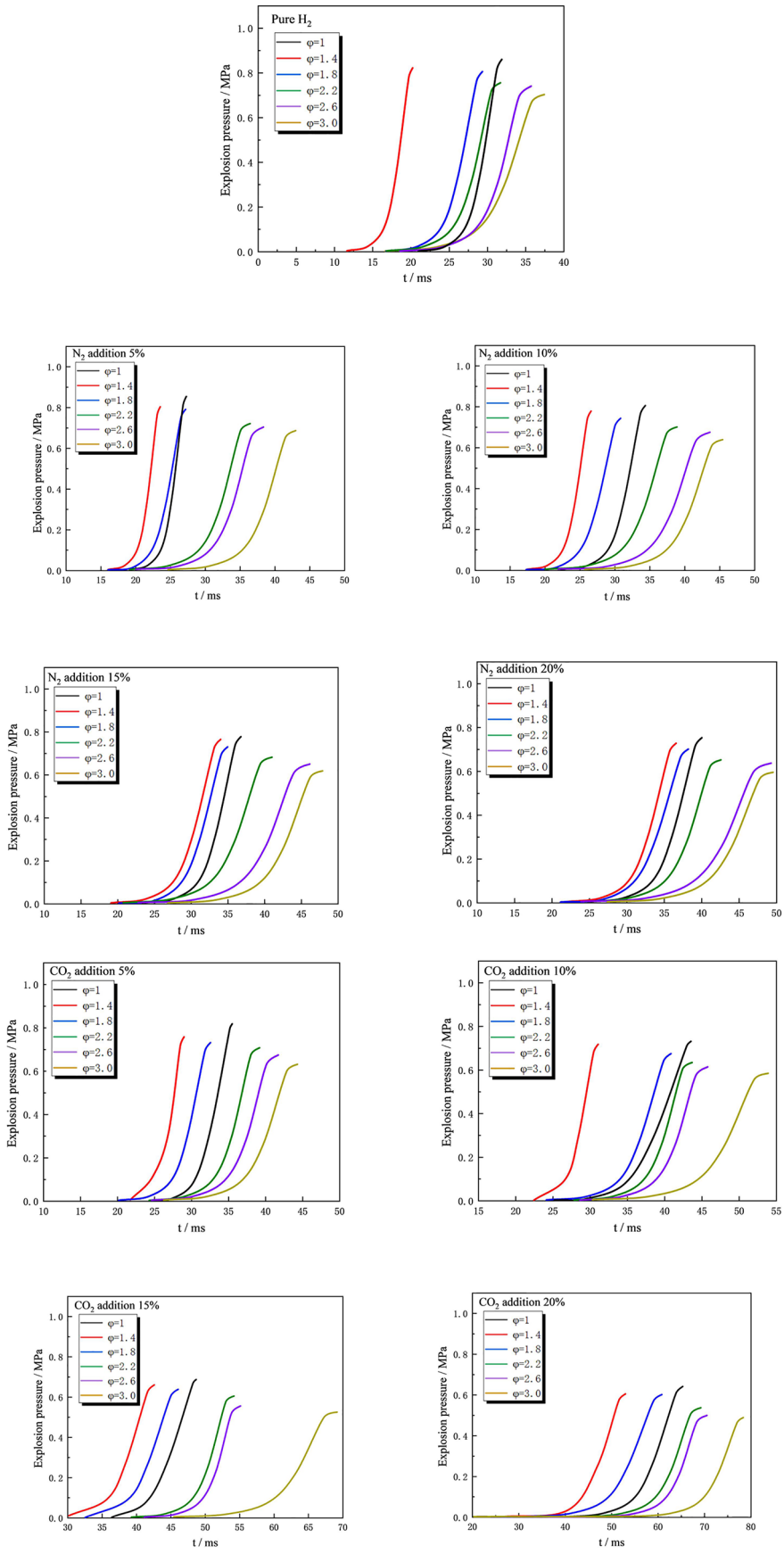

Figure 8. Plot of explosion pressure versus time.

https://doi.org/10.1021/acsomega.3c07631
ACS Omega 2023, 8, 48304−48316

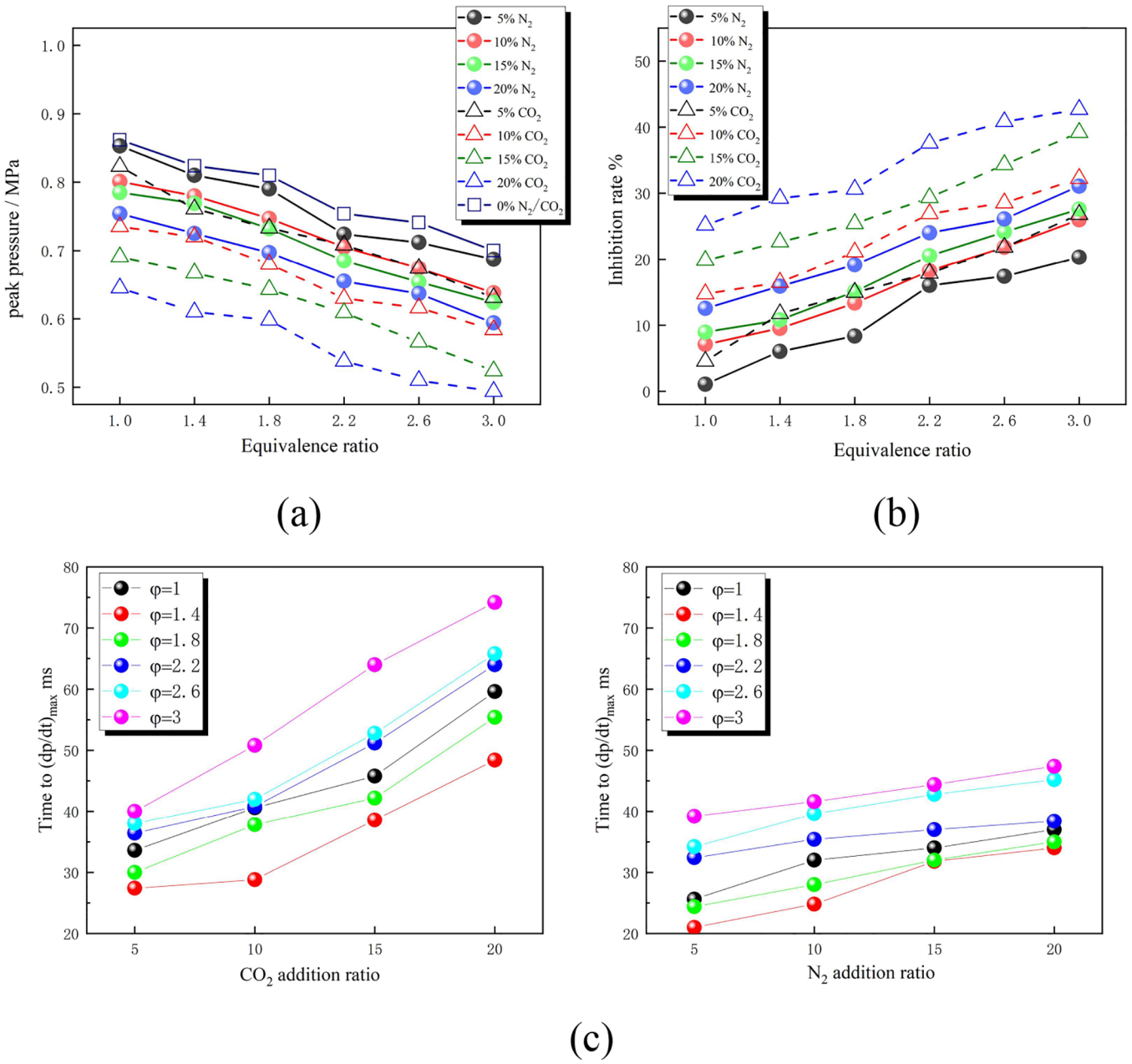

Figure 9. Explosion pressure peak variation curve and time to maximum pressure rise rate ((a) peak pressure variation curve with time; (b) decay rate of peak pressure; (c) time to the maximum pressure rise rate).

peaks with the addition of 10% CO_2. When φ is the same, CO_2 on the pressure peak inhibition range from 4.52 to 25.17%, N_2 on the pressure peak inhibition range from 1.04 to 12.53%, indicating that the influence of CO_2 inhibition is obviously better than N_2, and the inhibition efficiency is close to twice. The maximum suppression of the explosion pressure peak was 31.09% for N_2 additions up to 20%, which was close to the suppression of the pressure peak (32.25%) with the addition of 10% CO_2 at the same φ. The suppression of pressure peaks is evident with CO_2 additions above 15% and has a maximum suppression of 42.69% and a minimum suppression of 19.84%.

3.3. Sensitivity Analysis. A sensitivity analysis of the laminar flow flame velocity U_L was performed in order to explore the influence of N_2 and CO_2 on flame propagation at the basic reaction level. The sensitivity analysis was carried out using USC Mech II model, which solves the steady-state mass, species, and energy conservation equations using a hybrid time integration/Newtonian iteration technique.[56,57] The sensitivity coefficients of elemental reactions to laminar combustion rates for different φ under pure hydrogen conditions are listed in Figure 10. Among all equivalence ratios φ, the most important basic reaction to increasing the U_L is R1 ($H + O_2 = O + OH$). Table 2 lists the basic reactions and the corresponding number of steps. Regardless of the equivalence ratio φ, the reaction R1 always has the maximum sensitivity coefficient, and the reaction R12 ($H + O_2 + M = HO_2 + M$) has the lowest sensitivity coefficient. Since laminar combustion of hydrogen/air mixtures is strongly dependent on the concentration of H and OH radicals, OH and O radicals are formed in R1 despite the high consumption of H radicals, and the increase in φ enhances the chemical reactivity.

https://doi.org/10.1021/acsomega.3c07631
ACS Omega 2023, 8, 48304−48316

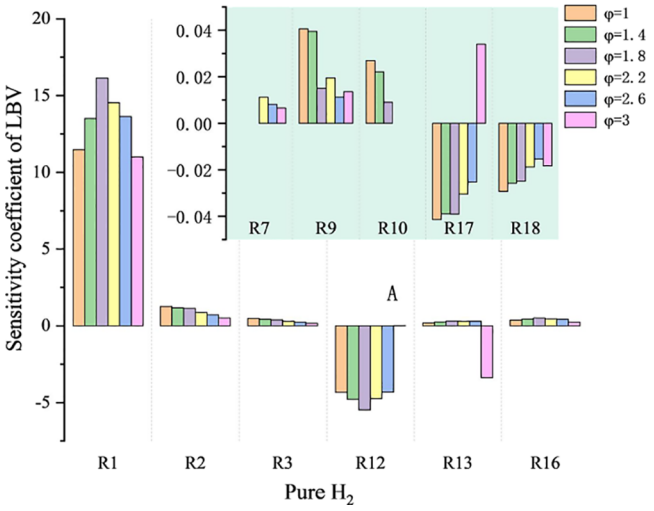

Figure 10. Sensitivity coefficients of elemental reactions to laminar combustion rates at different φ.

As shown in Figure 11, since N_2 does not participate in the oxidation reaction, only dilution and third body effects are accounted for, and the outcome shows that the dilution effect is mainly carried out through the R1 reaction, and the third effect is mainly carried out through the R12 reaction. In addition, CO_2 can participate in some of the chemical reactions. The main reaction in which CO_2 participates is the H-related reaction: R28 ($CO + OH = CO_2 + H$), and as the CO_2 equivalence ratio φ increases, the sensitivity coefficient of R28 basically tends to increase, but overall, the impact of R28 on the hydrogen combustion is comparatively small, which means that the chemical kinetics of CO_2 as a direct reactant and the third-body effects are small. In addition, thermal effects and diffusion factors also have an influence on laminar combustion. Due to the larger specific heat capacity of the diluent, which leads to a decrease in temperature, the velocity increases significantly with V_{Inert}. Compared with N_2, CO_2 has a higher specific heat capacity and a stronger thermal effect on the flame temperature. The dilution effect of CO_2 is therefore stronger and the decrease in laminar flame velocity is greater with increasing CO_2 concentration at the same dilution level. Compared to the thermal and chemical effects, the diffusivity change effect of the diluent is very small, and the reduction in laminar flame speed is negligible.

H and OH radicals play a crucial role in the critical chain reaction and are significantly correlated to the laminar flame velocity. Simulation results of H and OH molar fractions in premixed flames with different φ for 5 and 20% N_2 and CO_2 are given in Figure 12. According to the H_2 explosion chain reaction mechanism, large amounts of reactive radicals such as H and OH are generated throughout the explosion process, forming activation centers in the reaction chain, which in turn promote the explosion. During the gas explosion, the concentration of radicals that sustain the chain reaction is low, and the retention time is short. At the moment of explosion, the concentration of free radicals rises sharply to a peak due to energy build-up, and after the radicals collide, their concentration decreases rapidly and is then maintained at a stable value. Although OH is not as high as the H concentration, OH is still important because the molar fraction of OH is of a similar order of magnitude to that of H. From Figure 12, it is known that the peak of the molar fraction of H increases and then decreases as the φ increases, the peak of the molar fraction of OH gradually decreases, and the time to the maximum of H and OH increases. Comparing the molar fractions of H and OH radicals for the V_{Inert} of 20% N_2 and CO_2 it can be detected that the thermal and chemical kinetic functions of CO_2 cause a later generation of H and OH radicals, and that the partial chain reaction involving CO_2 causes a lower peak of H radicals than the peak of H radicals generated under N_2 atmosphere. Furthermore, in combination with the sensitivity coefficient results for the key element reactions, it can be observed that although the positive sensitivity coefficient for the chain reaction R1 decreases when $\varphi > 1.8$, R1 is still the main enhanced reaction with the largest positive sensitivity coefficient. The increase in the molar fraction of H promotes the chain reaction $H + O_2 = O + OH$ at a much faster reaction rate than the OH consumption rate. Thus, the increase in H not only promotes flame propagation but also leads to an increase in the OH molar fraction, which mainly promotes the oxidation of hydrogen. It is worth noting that the maximum production of H radicals does not show the same pattern of variation as the peak explosion pressure with increasing φ. This is because the explosion pressure value is a macroscopic feature generated by all elementary reactions in the system together, and the pattern of variation of the total production of a single radical does not represent the trend of the peak pressure, which is also illustrated in the literature.[51]

4. CONCLUSIONS

In the present work, the influence of different addition ratios V_{Inert} (5−20%) of N_2 and CO_2 gas on the characteristics of explosion flame and explosion pressure under high equivalence ratios φ (1.0−3.0) is systematically and experimentally studied, and the microscopic analysis is carried out by Chemkin. The experimental results showed that at high equivalence ratios, inert gas has little effect on flame stability. The addition of inert gas reduces the tensile rate in the early stage of flame growth. At high yield ratios, CO_2 inhibits explosive flame propagation twice as effectively as N_2. Due to the large heat capacity and chemical kinetic effects, CO_2 has a stronger

Table 2. Key Basic Reactions and Corresponding Step Counts

number	elementary reaction	number	elementary reaction
R1	$H + O_2 = O + OH$	R12	$H + O_2 + M = HO_2 + M$
R2	$O + H_2 = H + OH$	R13	$H_2 + O_2 = HO_2 + H$
R3	$OH + H_2 = H + H_2O$	R16	$HO_2 + H = OH + OH$
R5	$H + H + M = H_2 + M$	R17	$HO_2 + O = OH + O_2$
R7	$H + H + H_2O = H_2 + H_2O$	R18	$HO_2 + OH = O_2 + H_2O$
R9	$H + OH + M = H_2O + M$	R22	$H_2O_2 + H = HO_2 + H_2$
R10	$O + H + M = OH + M$	R28	$CO + OH = CO_2 + H$

https://doi.org/10.1021/acsomega.3c07631
ACS Omega 2023, 8, 48304−48316

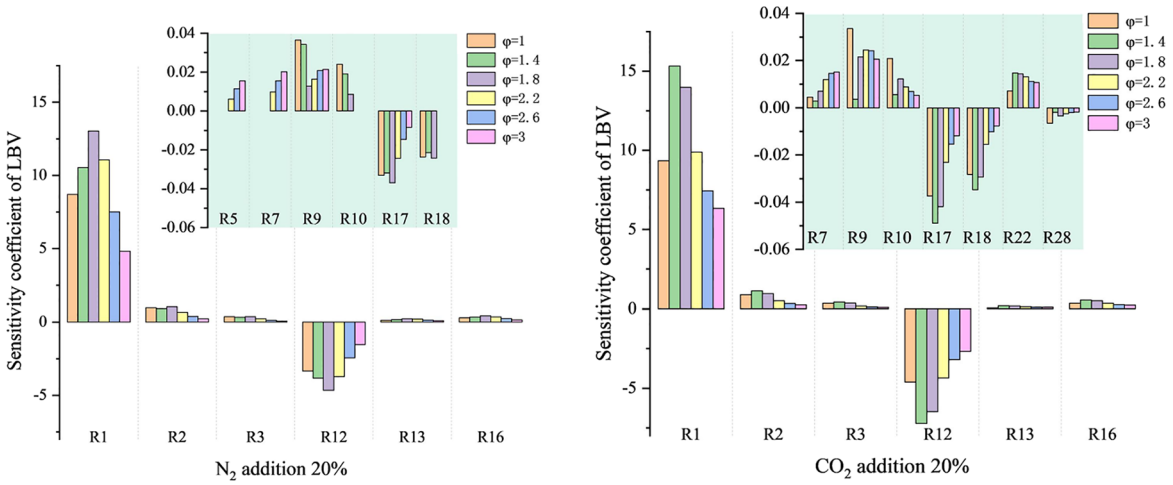

Figure 11. Sensitivity coefficients of elemental reactions to laminar combustion velocities at a V_{Inert} of 20%.

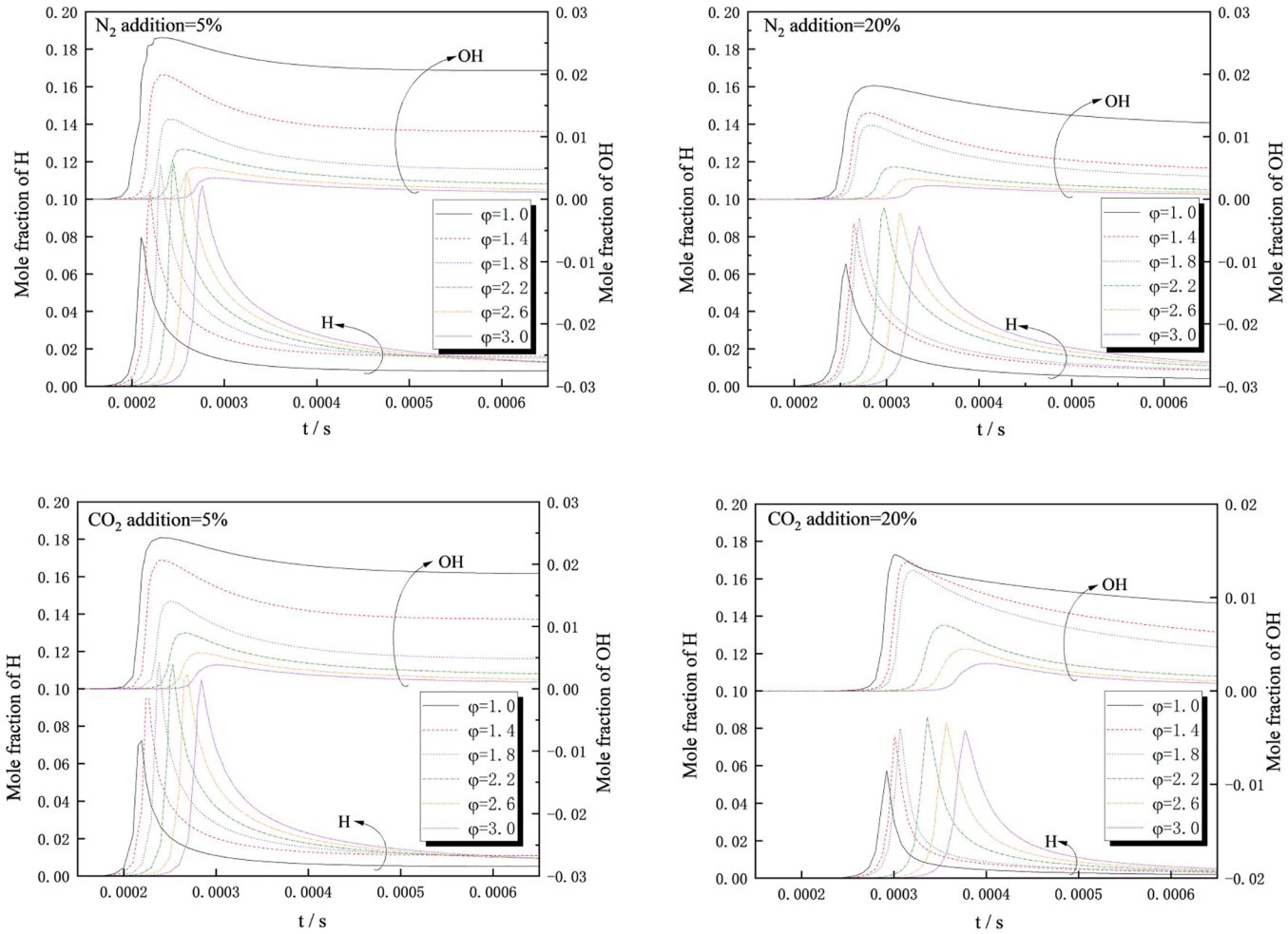

Figure 12. Simulation results of H and OH molar fractions for four different conditions.

inhibitory effect on the explosion pressure than N_2, and the inhibition efficiency on the explosion strength is nearly twice that high. To further analyze the effect of different inert gas addition ratios on chemical kinetics, sensitivity analysis and molar fraction simulations were performed. The thermal and chemical kinetic effects of CO_2 cause later generation of H and OH radicals and the partial chain reaction involving CO_2 causes a lower peak of H radicals than the peak of H radicals generated under the N_2 atmosphere. However, CO_2 is a direct reactant and the third body to produce a small chemical kinetic effect.

AUTHOR INFORMATION

Corresponding Author

Hao Qi − *School of Safety Science & Engineering, Xi'an University of Science and Technology, Xi'an, Shaanxi*

https://doi.org/10.1021/acsomega.3c07631
ACS Omega 2023, 8, 48304−48316

710054, P.R. China; orcid.org/0000-0002-7215-4127; Email: haoseven1314@163.com

Authors

Zhenmin Luo − *School of Safety Science & Engineering, Xi'an University of Science and Technology, Xi'an, Shaanxi 710054, P.R. China; Shaanxi Key Laboratory of Prevention and Control of Coal Fire, Xi'an, Shaanxi 710054, P.R. China; Shaanxi Engineering Research Center for Industrial Process Safety & Emergency Rescue, Xi'an, Shaanxi 710054, P.R. China;* orcid.org/0000-0001-5247-9656

Ruikang Li − *Postdoctoral Program, School of Energy, Xi'an University of Science and Technology, Xi'an, Shaanxi 710054, P.R. China*

Tao Wang − *School of Safety Science & Engineering, Xi'an University of Science and Technology, Xi'an, Shaanxi 710054, P.R. China; Shaanxi Engineering Research Center for Industrial Process Safety & Emergency Rescue, Xi'an, Shaanxi 710054, P.R. China;* orcid.org/0000-0002-1413-6270

Bin Su − *School of Safety Science & Engineering, Xi'an University of Science and Technology, Xi'an, Shaanxi 710054, P.R. China*

Yang Su − *College of Safety Science and Engineering, Henan Polytechnic University, Jiaozuo 454003, P.R. China*

Tianjun Zhang − *School of Safety Science & Engineering, Xi'an University of Science and Technology, Xi'an, Shaanxi 710054, P.R. China*

Complete contact information is available at: https://pubs.acs.org/10.1021/acsomega.3c07631

Author Contributions

Z.L.: Conceptualization, Methodology and Funding acquisition. H.Q.: Writing - Original Draft, software and Simulation. R.L.: Writing - Review and Editing. T.W.: Supervision. B.S.: Writing - Review & Editing. Y.S.: Data curation. T.Z.: Supervision.

Notes

The authors declare no competing financial interest.

■ ACKNOWLEDGMENTS

This work is supported by the National Key Research and Development Plan (Grant No. 2021YFB4000905), the Key Research and Development Plan of Shaanxi (No. 2023YBSF109), the National Natural Science Foundation of China (Nos. 52174200 and 52004208), the Innovation Capability Support Program of Shaanxi (No. 2020TD021), and the China Postdoctoral Science Foundation (No. 2023M732824).

■ REFERENCES

(1) Sharma, G. D.; Verma, M.; Taheri, B.; Chopra, R.; Parihar, J. S. Socio-economic aspects of hydrogen energy: An integrative review. *Technol. Forecast Soc. Change* **2023**, *192*, No. 122574.

(2) Luo, Z.; Zhou, S.; Wang, T.; Su, B.; Li, R. The weakening effect of the inhibition of CO_2 on the explosion of HCNG with the increase of hydrogen: Experimental and chemical kinetic research. *Int. J. Hydrogen Energy* **2023**, *48*, 32179.

(3) Zhao, T.; Chen, X.; Luo, Z.; Cheng, F.; Lu, K.; Shi, X.; et al. Effect of N_2 inerting on the inhibition of methane explosions by a multicomponent powder. *Fuel* **2023**, *337*, No. 127203.

(4) Liu, L.; Luo, Z.; Eckart, S.; Krause, H.; Wang, T.; Su, B.; et al. Investigation of C_2H_6, C_2H_4, CO and H_2 on the explosion pressure behavior of methane/blended fuels. *Int. J. Hydrogen Energy* **2023**, *48*, 27978.

(5) Jiang, B.; Yu, C.-F.; Yuan, L.; Lu, K.; Tao, W.; Lin, H.; Zhou, Y. Investigation on oxidative pyrolysis characteristics of bituminous coal through thermal analysis and density functional theory. *Applied Energy* **2023**, *349*, 121680.

(6) Wang, T.; Liang, H.; Luo, Z.; Yu, J.; Cheng, F.; Zhao, J.; et al. Thermal suppression effects of diluent gas on the deflagration behavior of H_2−air mixtures. *Energy* **2023**, *272*, No. 127146.

(7) Su, B.; Luo, Z.; Krietsch, A.; Wu, D.; Wang, T.; Zhou, S.; Deng, J. Quantitative investigation of explosion behavior and spectral radiant characteristics of free radicals for syngas/air mixtures. *International Journal of Hydrogen Energy* **2023**, DOI: 10.1016/j.ijhydene.2023.10.280.

(8) Su, B.; Luo, Z.; Deng, J.; Wang, T.; Liu, L.; Zhou, S.; et al. Comparative study on methane/air deflagration with hydrogen and ethane additions: Investigation from macro and micro perspectives. *Process Saf Environ. Prot* **2023**, *174*, 561−573.

(9) Wang, Q.; Jin, S.; Wen, H.; Luo, Z.; Shu, C.-M.; Gao, W.; et al. Dynamic characteristics of methane explosion flame propagation in three types of pipe. *Process Saf Environ. Prot* **2023**, *172*, 1029−1047.

(10) Wang, T.; Yi, W.; Liang, H.; Yang, P.; Luo, Z.; Sun, L.; et al. Experimental research on the pressure and flame propagation behaviors of LPG-air mixtures in a double obstructed tube. *J. Loss Prev Process Ind.* **2023**, *82*, No. 104979.

(11) Li, Y.; Yang, S.; Bi, M.; Zhou, Y.; Zhang, K.; Gao, W. Evaluation of hydrogen-blended methane explosion. *Int. J. Hydrogen Energy* **2023**, *48*, 31400.

(12) Liu, L.; Luo, Z.; Su, B.; Song, F.; Wu, P.; Wang, T.; Deng, J. Study on the explosion characteristics and flame propagation of hydrogen-methane-air mixtures in a closed vessel. *Journal of Loss Prevention in the Process Industries* **2024**, *87*, 105224.

(13) Wei, Z.; Liu, M.; Chen, Z.; Liu, Z.; Zhen, H. Numerical analysis on the combined transport effects of H_2 and CO_2 on the laminar premixed flame characteristics of biogas-hydrogen blends. *Int. J. Hydrog Energy* **2022**, *47*, 35484−35497.

(14) Wang, D.; Ji, C.; Wang, S.; Meng, H.; Yang, J. Chemical effects of CO_2 dilution on CH_4 and H_2 spherical flame. *Energy* **2019**, *185*, 316−326.

(15) Zhang, B.; Liu, H.; Li, Y. The effect of instability of detonation on the propagation modes near the limits in typical combustible mixtures. *Fuel* **2019**, *253*, 305−310.

(16) Zhang, B.; Liu, H. Theoretical prediction model and experimental investigation of detonation limits in combustible gaseous mixtures. *Fuel* **2019**, *258*, No. 116132.

(17) Guo, J.; Sun, X.; Rui, S.; Cao, Y.; Hu, K.; Wang, C. Effect of ignition position on vented hydrogen−air explosions. *Int. J. Hydrog Energy* **2015**, *40*, 15780−15788.

(18) Cao, Y.; Guo, J.; Hu, K.; Xie, L.; Li, B. Effect of ignition location on external explosion in hydrogen−air explosion venting. *Int. J. Hydrog Energy* **2017**, *42*, 10547−10554.

(19) Wang, L.-Q.; Ma, H.-H.; Shen, Z.-W. Effects of vessel height and ignition position upon explosion dynamics of hydrogen-air mixtures in vessels with low asymmetry ratios. *Fuel* **2021**, *289*, No. 119926.

(20) Huang, Z.; Zhang, Y.; Wang, Q.; Wang, J.; Jiang, D.; Miao, H. Study on Flame Propagation Characteristics of Natural Gas−Hydrogen−Air Mixtures. *Energy Fuels* **2006**, *20*, 2385−2390.

(21) Xie, Y.; Wang, X.; Wang, J.; Huang, Z. Explosion behavior predictions of syngas/air mixtures with dilutions at elevated pressures: Explosion and intrinsic flame instability parameters. *Fuel* **2019**, *255*, No. 115724.

(22) Hou, Y.; Liu, X.; Lei, M.; Lv, X.; Yu, X.; Yan, X.; et al. Detonation behaviors in stoichiometric CH_4-H_2-O_2 under different initial pressures conditions. *Fuel* **2023**, *349*, No. 128746.

(23) Bauwens, C. R.; Chao, J.; Dorofeev, S. B. Effect of hydrogen concentration on vented explosion overpressures from lean hydrogen−air deflagrations. *Int. J. Hydrog Energy* **2012**, *37*, 17599−17605.

(24) Bauwens, C. R.; Dorofeev, S. B. Effect of initial turbulence on vented explosion overpressures from lean hydrogen−air deflagrations. *Int. J. Hydrog Energy* **2014**, *39*, 20509−20515.
(25) Bauwens, C. R. L.; Bergthorson, J. M.; Dorofeev, S. B. Experimental investigation of spherical-flame acceleration in lean hydrogen-air mixtures. *Int. J. Hydrog Energy* **2017**, *42*, 7691−7697.
(26) Rudy, W. Transition to detonation in a hydrogen-air mixtures due to shock wave focusing in the 90 - deg corner. *Int. J. Hydrog Energy* **2023**, *48*, 12523−12533.
(27) Zhang, Y.; Cao, W.; Shu, C.-M.; Zhao, M.; Yu, C.; Xie, Z.; et al. Dynamic hazard evaluation of explosion severity for premixed hydrogen−air mixtures in a spherical pressure vessel. *Fuel* **2020**, *261*, No. 116433.
(28) Grune, J.; Sempert, K.; Kuznetsov, M.; Jordan, T. Experimental investigation of flame and pressure dynamics after spontaneous ignition in tube geometry. *Int. J. Hydrog Energy* **2014**, *39*, 20396−20403.
(29) Mogi, T.; Matsunaga, T.; Dobashi, R. Propagation of blast waves from a bursting vessel with internal hydrogen-air deflagration. *Int. J. Hydrog Energy* **2017**, *42*, 7683−7690.
(30) Ma, T.; Wu, D.; Li, J. Experimental study of the effect of a cavity on propagation behavior of premixed methane−air flame. *Fuel* **2023**, *338*, No. 127341.
(31) Wang, S.; Xiao, G.; Mi, H.; Feng, Y.; Chen, J. Experimental and numerical study on flame fusion behavior of premixed hydrogen/methane explosion with two-channel obstacles. *Fuel* **2023**, *333*, No. 126530.
(32) Cao, X.; Wei, H.; Wang, Z.; Wang, Y.; Fan, L.; Lu, Y. Effect of obstacle on the H_2/CO/Air explosion characteristics under lean-fuel conditions. *Fuel* **2022**, *319*, No. 123834.
(33) Luo, X.; Wang, C.; Rui, S.; Wan, Y.; Zhang, Z.; Li, Q. Effects of ignition location, obstacles, and vent location on the vented hydrogen-air deflagrations with low vent burst pressure in a 20-foot container. *Fuel* **2020**, *280*, No. 118677.
(34) Qiu, Y.; Xing, H.; Sun, S.; Wang, M.; Li, B.; Xie, L. Experimental study of the effects of vent area and ignition position on internal and external pressure characteristics of venting explosion. *Fuel* **2021**, *300*, No. 120935.
(35) Shang, R.; Zhuang, Z.; Yang, Y.; Li, G. Laminar flame speed of H_2/CH_4/air mixtures with CO_2 and N_2 dilution. *Int. J. Hydrog Energy* **2022**, *47*, 32315−32329.
(36) Su, Y.; Luo, Z.; Wang, T.; Chen, X.; Lu, K. Effect of nitrogen on deflagration characteristics of hydrogen/methane mixture. *Int. J. Hydrogen Energy* **2022**, *47*, 9156−9168.
(37) Wang, J.; Liang, Y.; Zhao, Z. Effect of N_2 and CO_2 on explosion behavior of H_2-Liquefied petroleum gas-air mixtures in a confined space. *Int. J. Hydrog Energy* **2022**, *47*, 23887−23897.
(38) Wang, L.-Q.; Ma, H.-H.; Shen, Z.-W. Explosion characteristics of hydrogen-air mixtures diluted with inert gases at sub-atmospheric pressures. *Int. J. Hydrog Energy* **2019**, *44*, 22527−22536.
(39) Li, Y.; Bi, M.; Huang, L.; Liu, Q.; Li, B.; Ma, D.; et al. Hydrogen cloud explosion evaluation under inert gas atmosphere. *Fuel Process. Technol.* **2018**, *180*, 96−104.
(40) Wei, H.; Xu, Z.; Zhou, L.; Zhao, J.; Yu, J. Effect of hydrogen-air mixture diluted with argon/nitrogen/carbon dioxide on combustion processes in confined space. *Int. J. Hydrog Energy* **2018**, *43*, 14798−14805.
(41) Zhang, S.; Wen, X.; Guo, Z.; Zhang, S.; Ji, W. Effect of N_2 and CO_2 on explosion behavior of hydrogen-air mixtures in non-premixed state. *Fire Saf J.* **2023**, *138*, No. 103790.
(42) Li, Y.; Bi, M.; Yan, C.; Liu, Q.; Zhou, Y.; Gao, W. Inerting effect of carbon dioxide on confined hydrogen explosion. *Int. J. Hydrog Energy* **2019**, *44*, 22620−22631.
(43) Yang, W.; Zheng, L.; Wang, C.; Wang, X.; Jin, H.; Fu, Y. Effect of ignition position and inert gas on hydrogen/air explosions. *Int. J. Hydrog Energy* **2021**, *46*, 8820−8833.
(44) Zhang, S.; Wen, X.; Guo, Z.; Zhang, S.; Ji, W. Experimental study on the multi-level suppression of N_2 and CO_2 on hydrogen-air explosion. *Process Saf Environ. Prot* **2023**, *169*, 970−981.
(45) Shang, R.; Zhuang, Z.; Niu, J.; Han, Q.; Li, G.; Zhang, P. Experimental study on the lower flammability limit of N_2 and CO_2 diluted H_2/CO/air mixtures at high initial pressure. *Int. J. Hydrog Energy* **2023**, *48*, 393−406.
(46) Zhang, G.-P.; Li, G.-X.; Li, H.-M.; Lv, J.-C. Experimental study on the effect of diluent gas on H_2/CO/air mixture turbulent premixed flame. *Int. J. Hydrog Energy* **2022**, *47*, 610−623.
(47) Yan, C.; Bi, M.; Li, Y.; Gao, W. Effects of nitrogen and carbon dioxide on hydrogen explosion behaviors near suppression limit. *J. Loss Prev Process Ind.* **2020**, *67*, No. 104228.
(48) Zhang, C.; Wen, J.; Shen, X.; Xiu, G. Experimental study of hydrogen/air premixed flame propagation in a closed channel with inhibitions for safety consideration. *Int. J. Hydrog Energy* **2019**, *44*, 22654−22660.
(49) Zhang, W.; Chen, Z.; Kong, W. Effects of diluents on the ignition of premixed H_2/air mixtures. *Combust. Flame* **2012**, *159*, 151−160.
(50) Bradley, D.; Gaskell, P. H.; Gu, X. J. Burning velocities, markstein lengths, and flame quenching for spherical methane-air flames: A computational study. *Combust. Flame* **1996**, *104*, 176−198.
(51) Luo, Z.; Li, D.; Su, B.; Wang, T.; Li, K.; Li, Q.; et al. Thermodynamic effects of the generation of H*/OH*/CH_2O* on flammable gas explosion. *Fuel* **2020**, *280*, No. 118679.
(52) Bradley, D.; Hicks, R. A.; Lawes, M.; Sheppard, C. G. W.; Woolley, R. The Measurement of Laminar Burning Velocities and Markstein Numbers for Iso-octane−Air and Iso-octane−n-Heptane−Air Mixtures at Elevated Temperatures and Pressures in an Explosion Bomb. *Combust. Flame* **1998**, *115*, 126−144.
(53) Leo, Y.; Zhang, B. Explosion behavior of methane-air mixtures and Rayleigh-Taylor instability in the explosion process near the flammability limits. *Fuel* **2022**, *324*, No. 124730.
(54) Li, J.; Zhao, Z.; Kazakov, A.; Dryer, F. L. An updated comprehensive kinetic model of hydrogen combustion. *Int. J. Chem. Kinet.* **2004**, *36*, 566−575.
(55) Davis, S. G.; Joshi, A. V.; Wang, H.; Egolfopoulos, F. An optimized kinetic model of H_2/CO combustion. *Proc. Combust Inst* **2005**, *30*, 1283−1292.
(56) Masri, A. R.; Dibble, R. W.; Barlow, R. S. Chemical Kinetic Effects in Nonpremixed Flames of H_2/CO_2 Fuel. *Combust. Flame* **1992**, *91* (3−4), 285−309.
(57) Jiang, B.; Ji, B.; Yuan, L.; Yu, C.-F.; Tao, W.; Zhou, Y.; Wang, H.; Wang, X.-H.; Liao, M. Experimental and molecular dynamics simulation study of the ionic liquids' chain-length on wetting of bituminous coal. *Energy* **2023**, *283*, 128507.

https://doi.org/10.1021/acsomega.3c07631
ACS Omega 2023, 8, 48304−48316